

## Supporting Information

### Superparamagnetic core-shell nanoparticles as solid supports for peptide synthesis

**Journal:** Chemical Communications

**Corresponding Author:** Hans G. Börner <sup>1</sup>

**Other Authors:** Christian Stutz,<sup>1</sup> Idalia Bilecka,<sup>2</sup> Andreas F. Thünemann,<sup>3</sup> Markus Niederberger<sup>2</sup>

<sup>1</sup> Humboldt-Universität zu Berlin, Department of Chemistry, Laboratory of Organic Synthesis of Functional Systems, Brook-Taylor-Str. 2, Berlin 12489, Germany,

E.mail: h.boerner@hu-berlin.de

Phone: +49 (0)30 2093 7348

Fax: +49 (0)30 2093 7500

<sup>2</sup> ETH Zürich, Department of Materials, Laboratory of Multifunctional Materials, Wolfgang-Pauli-Str. 10, Zürich 8093, Switzerland,

E.mail: markus.niederberger@mat.ethz.ch

Phone: +41 (0)44 633 63 90

Fax: +41 (0)44 633 15 45

<sup>3</sup> BAM Federal Institute for Materials Research and Testing, Unter den Eichen 87, Berlin 12205, Germany,

E Mail: andreas.thuenemann@bam.de

Phone: +49 (0)30 8104 1610

Fax: +49 (0)30 8104 1617

## Materials

*N*- $\alpha$ -Fmoc protected amino acid derivatives Fmoc- $\beta$ -Ala OH, Fmoc-Gly OH, Fmoc-Leu OH, Fmoc-Lys(Boc) OH, Fmoc-Phe OH, Fmoc-Arg(Pbf) OH, Fmoc-Asp(tBu) OH, Fmoc-Pro OH, Fmoc-Gln(Trt) OH, Fmoc-Trp(Boc) OH, Fmoc-Thr(tBu) OH, 4'-{(R,S)-alpha-[1-(9-Fluorenyl)methoxycarbonyl-amino]-2,4-dimethoxy-benzyl}-phenoxyacetic acid (Fmoc-Rink-Amid Linker), (benzotriazol-1-yloxy)-tripyrrolidinophosphonium-hexafluorophosphate (PyBOP) and *N*-methyl-2-pyrrolidone (NMP, 99.9+%, peptide synthesis grade) were used as received from IRIS Biotech GmbH (Marktredwitz, Germany). *N,N*-diisopropylethylamine (DIPEA; Sigma-Aldrich, 99%), piperidine (Acros, peptide grade), triethylsilane (TES; Alfa Aesar, Karlsruhe, Germany, 98+%) have been applied as received. Trifluoroacetic acid (TFA; Acros, peptide grade) was distilled prior use. Dichloromethane (DCM, IRIS Biotech GmbH, peptide grade) was distilled from CaH<sub>2</sub> prior use.

Iron(III) acetylacetonate (97%), anhydrous benzyl alcohol (99.8%) and (3-aminopropyl)trimethoxysilane were used as received from Sigma-Aldrich GmbH (Germany). Ammonia solution (25% in H<sub>2</sub>O) was used as received from Carl Roth GmbH (Karlsruhe, Germany). Ethanol absolute was used as received from VWR International (Darmstadt, Germany).

## Instrumentation and Methods

Particle synthesis, coating reactions and functionalization were carried out on a Discover SP-D Microwave by CEM GmbH (Kamp-Linfort).

Matrix-assisted laser desorption ionization time of flight mass spectroscopy (MALDI-TOF-MS) was performed on a Bruker Reflex III workstation. Peptides were dissolved in water at a final concentration of 0.1 mg/mL. 1  $\mu$ L of the sample solution was mixed with 1  $\mu$ L of the matrix solution, consisting of 10 mg of  $\alpha$ -cyano-4-hydroxy-cinnamic acid dissolved in 0.1 % TFA in acetonitrile-water (1:1, v/v), on the sample plate and air-dried at ambient temperature.

Measurements were performed in linear positive mode at an acceleration voltage of 20 kV with 30 shots per sample.

Liquid chromatography-mass spectrometry (HPLC-ESI-MS) was performed on an Agilent 1100 HPLC-System with UV/Vis-detector and VL-quadrupol mass spectrometer (Agilent Technologies Germany GmbH). A temperature-controlled column (55°C, RP-C18, Polaris, Germany) was used. Detection was carried out at a wavelength of  $\lambda=210$  nm. A mixture of eluent A (water, 1 % acetonitrile, 0.1 % formic acid) and eluent B (acetonitrile, 1 % water, 0.1 % formic acid) with a flow rate of  $0.3 \text{ mL}\cdot\text{min}^{-1}$  was used for elution with the following gradient: 3-50 % of B in 20 min.

$^1\text{H}$  nuclear magnetic resonance spectrum ( $^1\text{H-NMR}$ ) was recorded on a Bruker AV 500 spectrometer at 500 MHz in TFA- $\text{d}_1$  at room temperature.

Fourier transform infrared spectroscopy (ATR-FT-IR) was conducted on a JASCO FT/IR-4200 Fourier transform infrared spectrometer (Golden gate) in a range of  $500 - 4000 \text{ cm}^{-1}$ . Samples were measured in solid form at room temperature.

Transmission electron microscopy (TEM) measurements were performed on a Philips Tecnai F30 microscope at 300 kV. One drop of an ethanol suspension was deposited on a carbon-coated copper grid. To minimize agglomeration of the nanoparticles the copper grid was placed on a filter paper during air drying.

Scanning electron microscopy (SEM) measurements were performed on a LEO 1530 Gemini operated at 5 kV. The particles were diluted in ethanol and air-dried at ambient temperature on an aluminum-plate.

Atomic force microscopy (AFM) measurements were performed on a Multimode 8 scanning probe microscope (Bruker, Santa Barbara California) in tapping mode<sup>TM</sup> using a MPP-11120-10 premium high resolution tapping mode silicon probes (Bruker, California USA).

Absorption measurements were performed on a Shimadzu UV-VIS recording spectrophotometer UV-2501PC using quartz cells.

Small-Angle X-ray Scattering (SAXS) measurements of dispersions of  $\text{Fe}_3\text{O}_4@\text{SiO}_2@\text{NH}-(\beta\text{Ala})_2@\text{Rink-Linker}$  particles were performed at the *BAMline* at the synchrotron BESSY II (Berlin, Germany) with a Kratky-type instrument (SAXSess from Anton Paar, Austria) at  $25 \pm 1^\circ \text{C}$ . The SAXSess has a low sample-to-detector distance (0.309 m), which is appropriate for investigation of dispersions with low scattering intensities. The measured intensity was corrected by subtracting the intensity of a capillary filled with pure solvent. The scattering vector is defined in terms of the scattering angle  $\theta$  and the wavelength  $\lambda$  of the radiation ( $\lambda = 0.124 \text{ nm}$ ): thus  $q = 4\pi/\lambda \sin\theta$ . Deconvolution (slit length desmearing) of the SAXS curves was performed with SAXSquant software (Anton Paar).

The Brunauer-Emmett-Teller (BET) surface area was measured on a Quadrasorb SI-MP from QUANTACHROME and calculated by multiple-point measurement in the relative pressure range of 0.05-0.15.

X-ray powder diffraction studies (XRD) were performed on a Philips PW 1800 diffractometer in reflection mode using  $\text{Cu K}\alpha$   $\lambda = 1.5406 \text{ \AA}$  radiation and a post sample monochromator.

Magnetic sedimentation of the particles was performed with Neodymium-Iron-Boron (NdFeB) magnets from Webcraft GmbH (Gottmadingen, Germany) with a remanence of 1.26-1.29 T.

## SYNTHESIS AND ANALYSIS

### Synthesis of core-shell nanoparticles

#### *Synthesis of Fe<sub>3</sub>O<sub>4</sub> particles*

0.4 mmol of iron (III) acetylacetonate were put into a 10 mL glass tube sealed with a Teflon cap and dissolved in 4 mL of benzyl alcohol in a glove box under inert atmosphere ( $O_2$  and  $H_2O < 0.1$  ppm). The reaction mixture was heated in a microwave reactor operating at 2.45 GHz to a temperature of 170°C and kept at this temperature for another 12 min with a maximum operating power of 300 W. After the reaction the solution was thermally quenched by compressed air and the suspension was separated from the liquid phase by magnetic sedimentation. The precipitate was washed with ethanol twice, dispersed in 8 mL ethanol absolute and used in coating reactions.

Zeta-potential (electric-potential difference between the dispersion medium and the stationary layer of fluid attached to the dispersed particle) displayed a value of +44.26 mV.

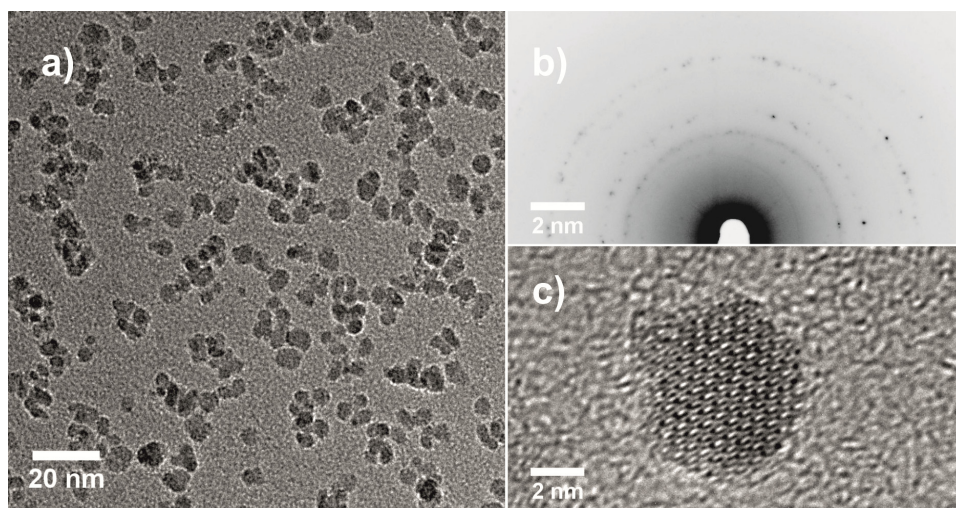


Figure S1. a) TEM overview of Fe<sub>3</sub>O<sub>4</sub> particles, b) electron diffraction of a large zone and c) HRTEM of a unique single-crystal particle.

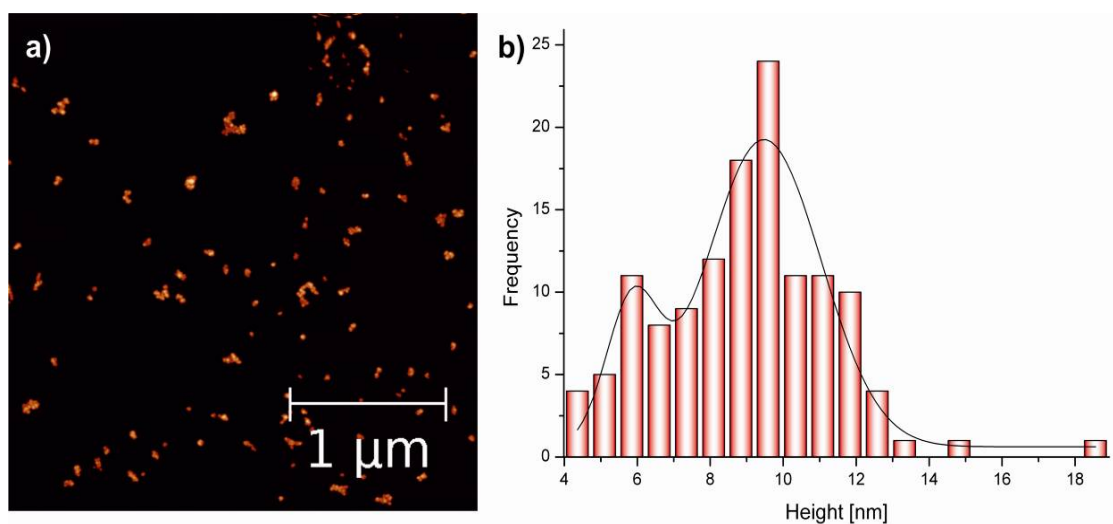


Figure S2. a) AFM overview of  $\text{Fe}_3\text{O}_4$  particles ( $z_{\text{max}}=20$  nm) on Mica sheet (V1 Quality, 50x75mm, 0.16 mm thick) and b) height-distribution.

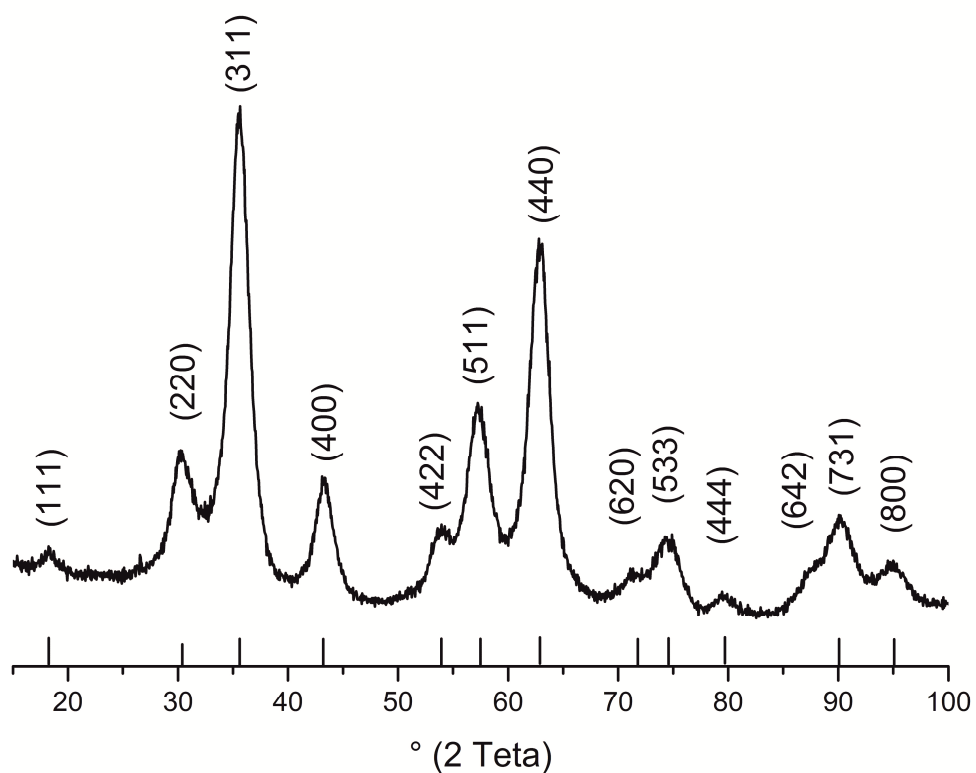


Figure S3. Experimental XRD pattern of the  $\text{Fe}_3\text{O}_4$  powder with the calculated magnetite pattern as vertical bars (ICDD PDF No. 19-629).

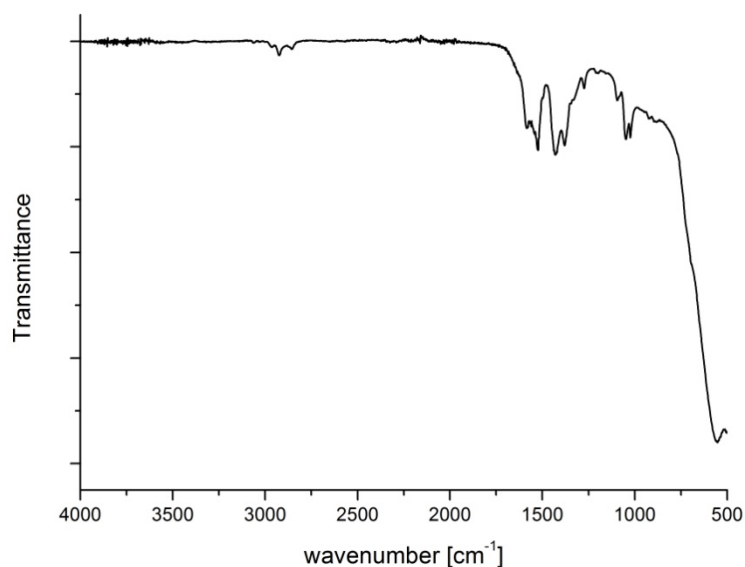


Figure S4. IR-spectrum of  $\text{Fe}_3\text{O}_4$  particles.

FT-IR ( $\nu(\text{cm}^{-1})$ ): 2932 (w, benzyl alcohol), 1591 (m, benzyl alcohol), 1529 (m, benzyl alcohol), 1435 (m, benzyl alcohol), 1385 (m, benzyl alcohol), 1053 (w, benzyl alcohol), 1026 (w, benzyl alcohol), 570 (s, Fe-O stretching vibration).

#### *Synthesis of $\text{Fe}_3\text{O}_4@Si\text{O}_2$ particles*

4 mL of dispersed  $\text{Fe}_3\text{O}_4$  particles in ethanol were put into a 10 mL glass tube. 1500  $\mu\text{L}$  water (~16.5 M), 225  $\mu\text{L}$  (1 mmol) tetraethyl orthosilicate and 180  $\mu\text{L}$  ammonia solution (25 % in  $\text{H}_2\text{O}$ ) (~0.5 M) were added and the tube sealed with a Teflon cap. The reaction mixture was heated in a microwave reactor to a temperature of 60°C and kept at this temperature for another 3 min with a maximum operating power of 300 W. After the reaction the solution was thermally quenched by compressed air and the suspension was separated from the liquid phase by magnetic sedimentation. The precipitate was washed with ethanol twice and used for amino functionalization.

Zeta-potential data displayed a value of -38.08 mV.

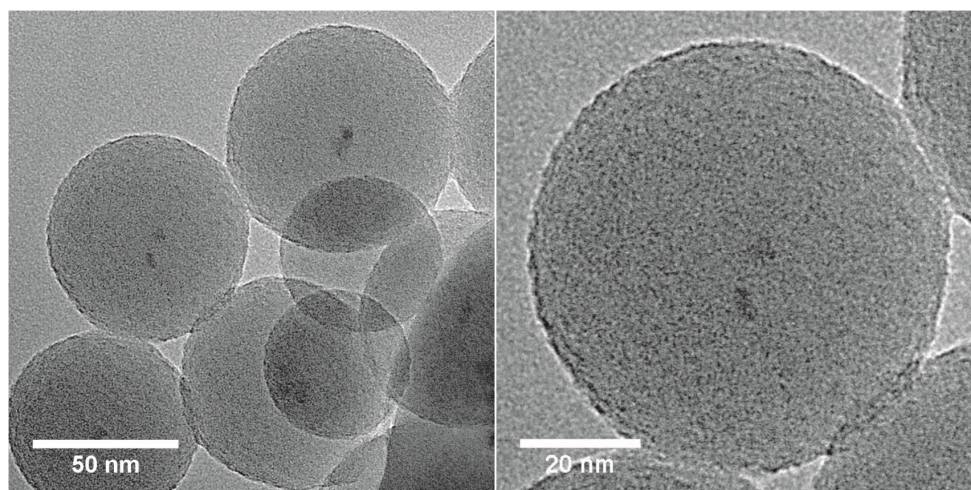


Figure S5. Transmission electron microscopy (TEM) images showing  $\text{Fe}_3\text{O}_4@\text{SiO}_2$  colloids. The  $\text{Fe}_3\text{O}_4$  particles are embedded in the center of the  $\text{SiO}_2$  matrix.

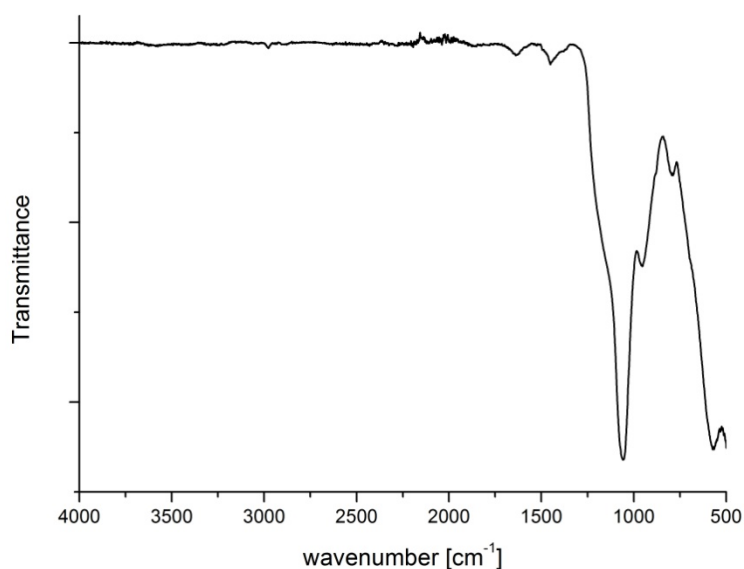


Figure S6. IR-spectrum of  $\text{Fe}_3\text{O}_4@\text{SiO}_2$  particles.

FT-IR ( $\nu(\text{cm}^{-1})$ ): 1462 (w, benzyl alcohol), 1070 (s,  $\text{SiO}_2$  stretching vibration), 986 (m,  $\text{SiO}_2$ ), 806 (m,  $\text{SiO}_2$  bending vibration), 586 (s, Fe-O stretching vibration).

#### *Synthesis of $\text{Fe}_3\text{O}_4@\text{SiO}_2@\text{NH}_2$ particles*

$\text{Fe}_3\text{O}_4@\text{SiO}_2$  particles were dispersed in 4 mL of ethanol and put into a 10 mL glass tube. 1500  $\mu\text{L}$  water ( $\sim 16.5$  M), 225  $\mu\text{L}$  (1 mmol) tetraethyl orthosilicate and 180  $\mu\text{L}$  ammonia solution (25 % in  $\text{H}_2\text{O}$ ) ( $\sim 0.5$  M) were added and the tube sealed with a Teflon cap. The reaction mixture was heated in a microwave reactor to a temperature of  $60^\circ\text{C}$  and kept at this temperature for another 3 min with a maximum operating power of 300 W. After the reaction the solution was thermally quenched by compressed air and the suspension was separated

from the liquid phase by magnetic sedimentation. The precipitate was washed with ethanol twice and used for peptide synthesis.

Zeta-potential data displayed a value of +41.14 mV.

BET-measurement of the particles resulted in a surface of 29.72 m<sup>2</sup>/g.

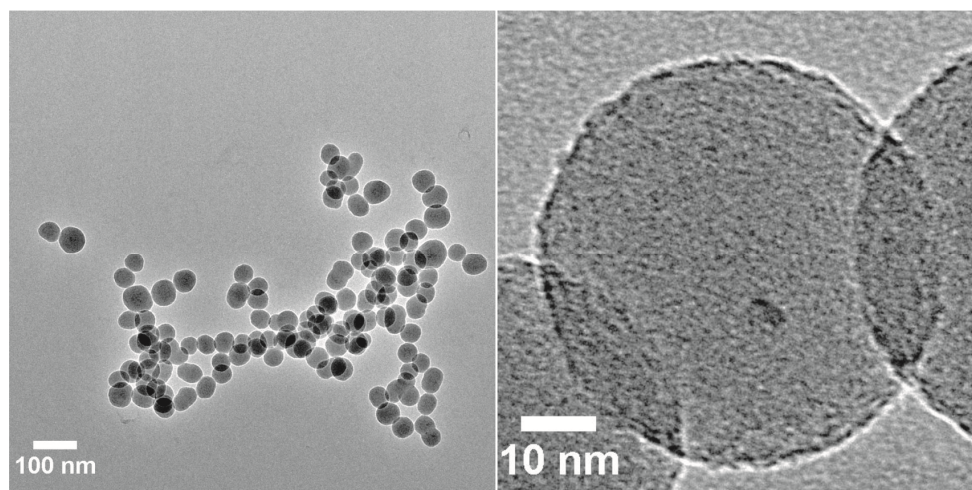


Figure S7. Transmission electron microscopy (TEM) showing amino-functionalized Fe<sub>3</sub>O<sub>4</sub>@SiO<sub>2</sub>@NH<sub>2</sub> colloids. Fe<sub>3</sub>O<sub>4</sub> particles embedded in SiO<sub>2</sub>@NH<sub>2</sub> matrix.

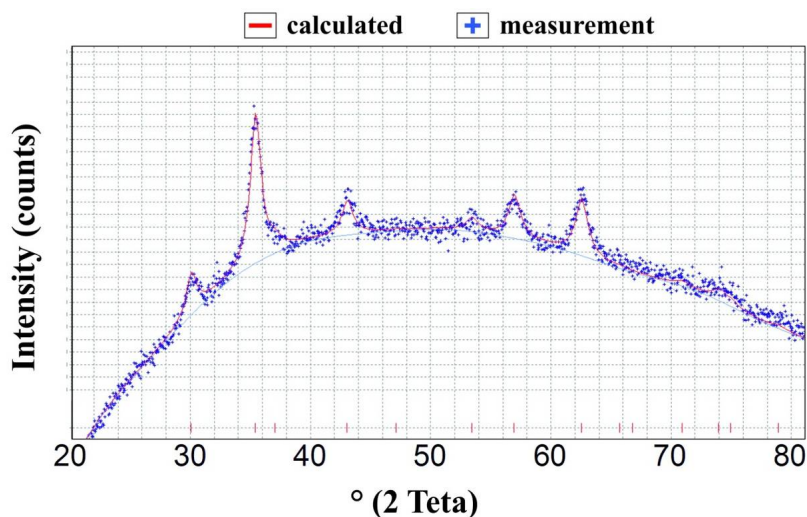


Figure S8. WAXS pattern of Fe<sub>3</sub>O<sub>4</sub>@SiO<sub>2</sub>@NH<sub>2</sub> particles corresponds to a calculated magnetite pattern. The size of magnetite crystals is around 9 nm calculated with Scherrer equation.

Table S1. Energy-dispersive X-ray spectroscopy (EDX) measurements: background corrected elemental composition of  $\text{Fe}_3\text{O}_4$ ,  $\text{Fe}_3\text{O}_4@\text{SiO}_2$  and  $\text{Fe}_3\text{O}_4@\text{SiO}_2@\text{NH}_2$  nanoparticles

particles	O	Fe	Si	C	N
$\text{Fe}_3\text{O}_4$	38%	62%	n.d.	n.d.	n.d.
$\text{Fe}_3\text{O}_4@\text{SiO}_2$	71%	16%	13%	n.d.	n.d.
$\text{Fe}_3\text{O}_4@\text{SiO}_2@\text{NH}_2$	62%	7%	4%	22%	5%

n.d.=not detected

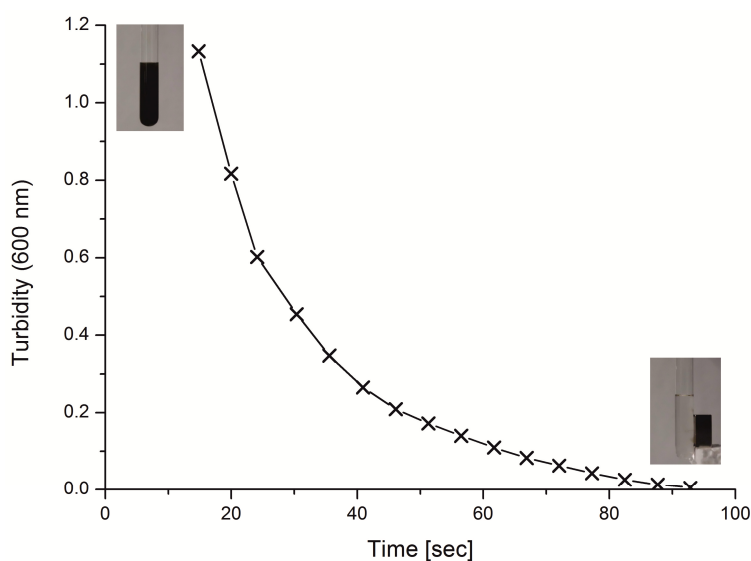


Figure S9. Turbidity measurements following magnetic sedimentation of  $\text{Fe}_3\text{O}_4@\text{SiO}_2$  particles in e.g. ethanol.

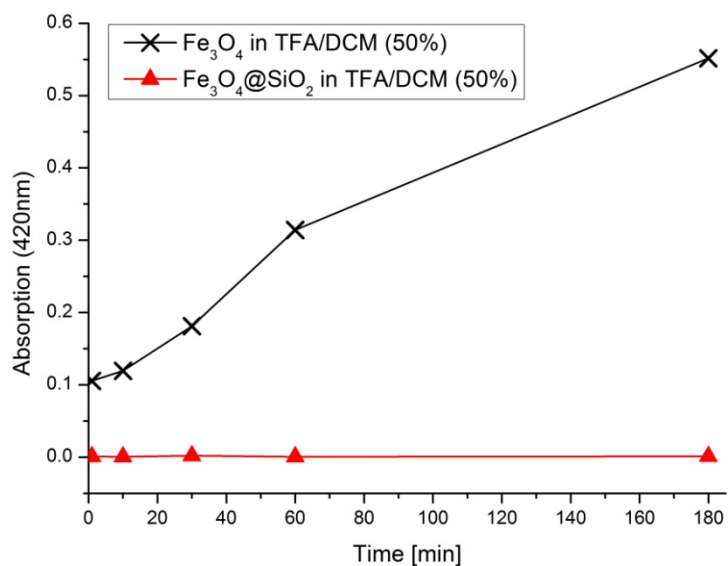


Figure S10. UV measurements ( $\lambda=420\text{ nm}$ ) following stability of  $\text{Fe}_3\text{O}_4$  and  $\text{Fe}_3\text{O}_4@\text{SiO}_2$  particles in a solution of 50 % TFA in DCM.

## Organic functionalization and peptide synthesis

### *Coupling of Fmoc-β-Ala OH and Fmoc-Rink-Amid Linker*

$\text{Fe}_3\text{O}_4@\text{SiO}_2@\text{NH}_2$  particles were dispersed in a solution of 93 mg (300  $\mu\text{mol}$ ) Fmoc- $\beta$ -Ala OH, 156 mg (300  $\mu\text{mol}$ ) PyBOP and 157  $\mu\text{L}$  (900  $\mu\text{mol}$ ) DIPEA in 10 mL NMP. The reaction mixture was stirred overnight and separated from the solid support by magnetic sedimentation. After removal of the protecting group using a solution of piperidine in NMP (20%) the reaction was repeated. The observed  $\text{Fe}_3\text{O}_4@\text{SiO}_2@\text{NH}-(\beta\text{Ala})_2$  particles were dispersed in a solution of 162 mg (300  $\mu\text{mol}$ ) Fmoc-Rink-Amid Linker, 156 mg (300  $\mu\text{mol}$ ) PyBOP and 157  $\mu\text{L}$  (900  $\mu\text{mol}$ ) DIPEA in 10 mL NMP. The reaction mixture was stirred overnight and separated from the solid support by magnetic sedimentation. The particles were washed with NMP and DCM and used for standard peptide synthesis. Quantitative Fmoc-analysis after deprotection using a solution of piperidine in NMP (20%) resulted in a concentration of 0.11 mmol free amino groups per gram particles.

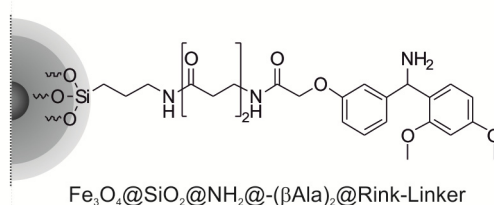


Figure S11. Structure of  $\text{Fe}_3\text{O}_4@\text{SiO}_2@\text{NH}-(\beta\text{Ala})_2@\text{Rink-Linker}$  particles.

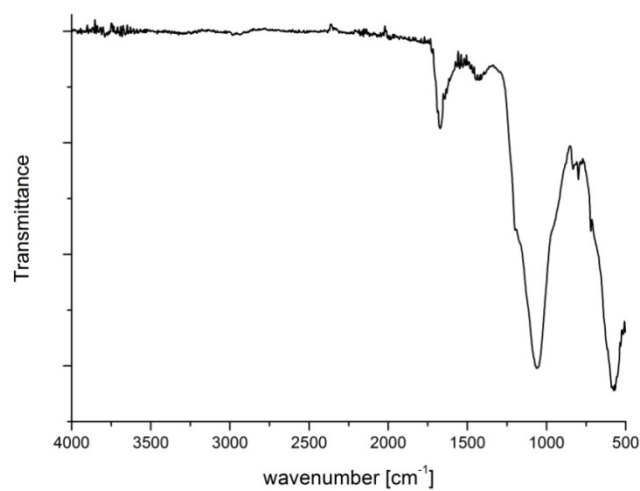


Figure S12. IR-spectrum of Fe<sub>3</sub>O<sub>4</sub>@SiO<sub>2</sub>@NH-(βAla)<sub>2</sub>@Rink-Linker particles.

FT-IR ( $\nu(\text{cm}^{-1})$ ): 1672 (w, Amid), 1548 (w, Amid), 1339 (w, C-H deformation vibration), 1190 (m, SiO<sub>2</sub>), 1063 (s, SiO<sub>2</sub>), 850 (w, H<sub>Ar</sub>), 771 (w, H<sub>Ar</sub>), 713 (m, C<sub>Ar</sub>), 580 (s, Fe-O stretching vibration).

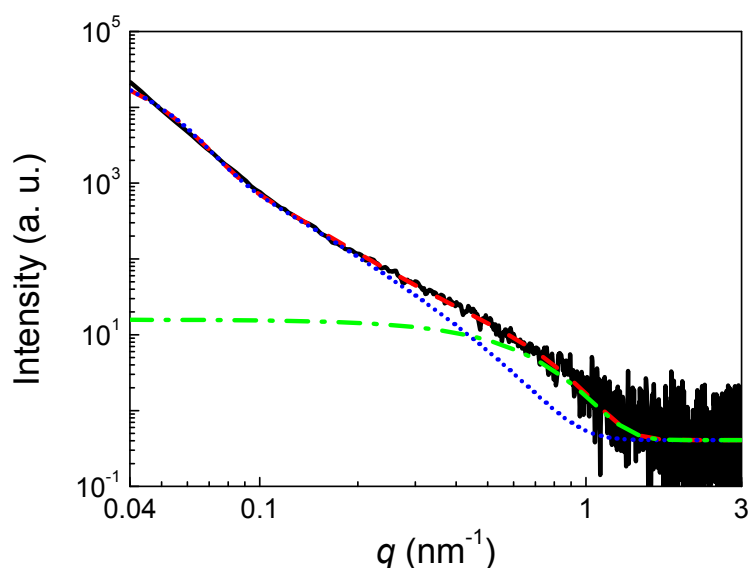


Figure S13. SAXS results from dispersions of  $\text{Fe}_3\text{O}_4@\text{SiO}_2@\text{NH}-(\beta\text{Ala})_2@\text{Rink-Linker}$  particles. Solid lines are measured data and dotted lines are curve fits according to the unified exponential/power law. Scattering contributions of  $\text{Fe}_3\text{O}_4$ -cores and  $\text{SiO}_2$ -shells are given (dash-dotted and dotted line, respectively).

Probing of the *in situ* nanoparticles' structure was carried out with SAXS on a length scale between  $\pi/q_{\text{max}} = 1 \text{ nm}$  and  $\pi/q_{\text{min}} = 80 \text{ nm}$ . The resulting scattering pattern of  $\text{Fe}_3\text{O}_4@\text{SiO}_2@\text{NH}-(\beta\text{Ala})_2@\text{Rink-Linker}$  particles is shown in Figure S14 (solid line). It can be seen from the shape of the curve that the second shell with the  $\text{NH}-(\beta\text{Ala})_2@\text{Rink-Linker}$  cannot be seen with SAXS. This must be expected because the X-ray scattering contrast of the organic material in the  $\text{NH}_2$ -shell is approximately two orders of magnitude lower than that of the inorganic  $\text{SiO}_2$ -shell and moreover the  $\text{Fe}_3\text{O}_4$ -core. The curve displays a defined Guinier region at  $q$ -values below  $0.07 \text{ nm}^{-1}$  which proves the presence of defined nanoparticles and the absence of aggregates. The intensities characteristically scale with  $q^{-2.6}$  in the region around  $q = 0.2 \text{ nm}^{-1}$  and with  $q^{-4}$  at  $1.0 \text{ nm}^{-1}$ . The  $q^{-4}$  intensity decay is the classical Porod law,<sup>1</sup> as must be valid for  $\text{Fe}_3\text{O}_4$  nanoparticles with a sharp density transition between a  $\text{Fe}_3\text{O}_4$ -core and its  $\text{SiO}_2$  surroundings. In contrast to the  $\text{Fe}_3\text{O}_4$  particles' core, the  $q^{-2.6}$  decay in the medium  $q$ -region is typical for a mass fractal structure. Here we explain the absence of a second  $q^{-4}$ -scaling as resulting from a nonhomogeneous structure of the  $\text{SiO}_2$ -shell which in

addition has a roughened surface as can be seen on the electron micrograph pictures. We were not able to fit the curves sufficiently with simple concentric core-shell model curves that require homogeneous densities of shell and core.<sup>2</sup> These models produce significant deviations in the region around  $q = 0.2 \text{ nm}^{-1}$  as must be expected from an inhomogeneous shell density.

A quantitative description of the SAXS curves is possible by applying the Beaucage model that has been developed for nanosystems with different levels of hierarchical organization<sup>3</sup>. The characteristics of the scattering of a nanoparticle composed of small cores and a large shell should be describable in the functional form of two Guinier ( $I(q) = G \exp[-\frac{1}{3} R_g^2 q^2]$ ) and two power law regions ( $I(q) = Bq^{-P}$ ). Beaucage introduced a way how a smooth transition between Guinier and power law region could be realized which is named the unified exponential/power-law.<sup>3</sup> Therein Guinier and power law regimes are combined for an arbitrary number of structural levels. Applying this approach, we have two interrelated hierarchical levels, i.e. the level of the large inhomogeneous shell and the level of the small  $\text{Fe}_3\text{O}_4$  cores (labeled as 1 and 2, respectively). The scattering intensity for this two-level morphology is given by

$$I(q) = G_1 \exp\left(-\frac{q^2 R_{g,1}^2}{3}\right) + B_1 \exp\left(-\frac{q^2 R_{g,1}^2}{3}\right) \left\{ \left[ \text{erf}\left(q R_{g,1} \sqrt{6}^{-\frac{1}{2}}\right) \right]^3 q^{-1} \right\}^{p_1} + G_2 \exp\left(-\frac{R_{g,2}^2 q^2}{3}\right) + B_2 \left\{ \left[ \text{erf}\left(q R_{g,2} \sqrt{6}^{-\frac{1}{2}}\right) \right]^3 q^{-1} \right\}^{p_2} + bkg$$

Therein the Guinier radius of gyration of the  $\text{SiO}_2$ -shell is  $R_{g,1}$  and that of the  $\text{Fe}_3\text{O}_4$  cores is  $R_{g,2}$ . Guinier prefactors are  $G_1$  and  $G_2$ . For the power law, the prefactors are  $B_1$  and  $B_2$ , the power exponents are  $p_1$  and  $p_2$ . Some remaining background scattering resulting from density fluctuations is considered as constant  $bkg$ .

The scattering data are well-described by the unified exponential/power law as can be seen in Figure S14 (solid and dashed lines, respectively). Therein, for  $\text{Fe}_3\text{O}_4@SiO_2@NH-(\beta\text{Ala})_2@Rink\text{-Linker}$  the scattering contributions from the  $\text{Fe}_3\text{O}_4$  cores and from the  $\text{SiO}_2$  are

given exemplarily (dotted and dash-dotted line, respectively). The determined  $\text{Fe}_3\text{O}_4$  core radii of gyration are  $(2.7 \pm 0.1)$  nm. The width of the cores' size distribution was estimated to approximately 10 % according to Beaucage.<sup>4, 5</sup> The core diameters are  $(6.9 \pm 0.3)$  nm when calculating the diameters as  $D = 2 \times (5/3)^{1/2} R_g$  for simple comparison with our TEM results. Indeed, these sizes are in good agreement with the TEM data. The shells' radii of gyration are  $(45 \pm 1)$  nm. The size distributions of the shells are much broader than those of the cores but cannot be determined because the shells display no Porod law.<sup>5</sup> The intensity weighted  $\text{SiO}_2$  shell diameters are approximately 110 nm. These are larger than the number weighted diameters derived from TEM. But SAXS and TEM results are in agreement when taking into account that the intensity-weighted diameter must be larger than the number-weighted for disperse samples. The  $p_1$  value is  $2.58 \pm 0.03$  from which it can be concluded that the  $\text{SiO}_2$ -shell structure is inhomogeneous. Note that  $p_2$  was held constant at 4 to prevent unambiguous fit results.

### Peptide Synthesis

#### Synthesis of H<sub>2</sub>N-Phe-Lys-Leu-Gly-CONH<sub>2</sub>

Standard Fmoc-amino acids were coupled on support via standard protocol (single coupling, no capping) in an Erlenmeyer flask. Peptide synthesis was performed in NMP using Fe<sub>3</sub>O<sub>4</sub>@SiO<sub>2</sub>@NH-(βAla)<sub>2</sub>@Rink-Linker-particles as solid support. Fmoc-amino acid coupling was facilitated by PyBOP/DIPEA. An external magnetic field was used to separate the solid support reversible from the liquid reaction mixture (sedimentation time: 5 min). After final Fmoc removal the peptide was cleaved from the particles with 50:50 v/v TFA-DCM two times for 3 h resulting in the fully deprotected peptide, which was purified in diethyl ether. The synthesis yielded in 1.9 mg of the peptide with 95 % purity.

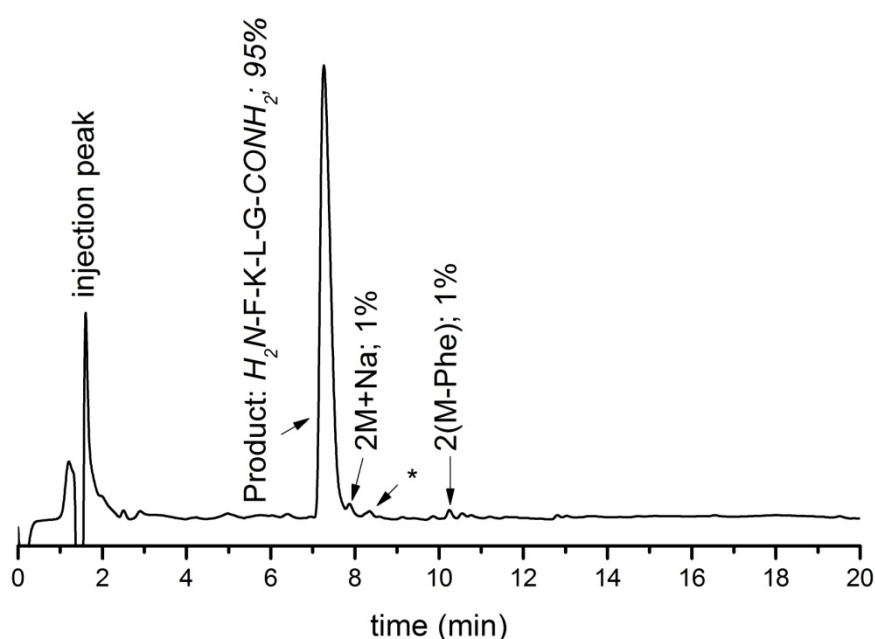


Figure S14. HPLC-trace of synthesized peptide H<sub>2</sub>N-Phe-Lys-Leu-Gly-CONH<sub>2</sub> (gradient: 3 - 50 % MeCN, RP-C<sub>18</sub>-column, λ=210 nm; \* = no mass detected).

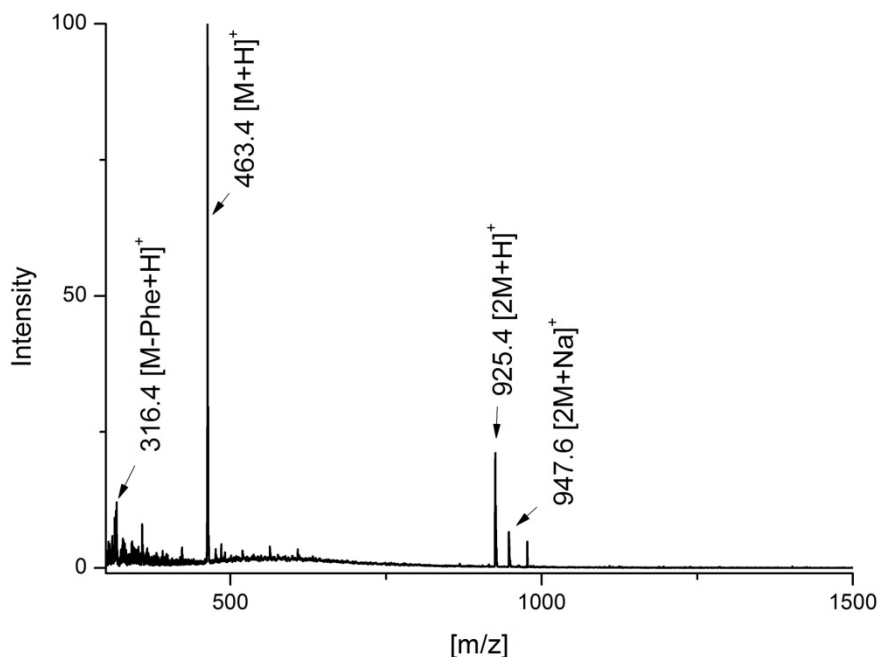


Figure S15. ESI-MS-spectrum of synthesized peptide  $\text{H}_2\text{N-Phe-Lys-Leu-Gly-CONH}_2$ .  
 $m/z$  (%):  $M_{\text{Th}} = 462.29$  g/mol: 316.4 (9) ( $[\text{M-Phe+H}]^+$ ); 463.4 (100) ( $[\text{M+H}]^+$ ); 925.4 (21) ( $[\text{2M+H}]^+$ ); 947.6 (7) ( $[\text{2M+Na}]^+$ ).

$^1\text{H}$  NMR (500 MHz, TFA-d,  $\delta$  in ppm): 7.46-7.29 (m, 5H,  $\text{CH}_{\text{Ar}}$  Phe), 4.84-4.73 (m, 2H,  $\text{C}^\alpha\text{H}$  Leu,  $\text{C}^\alpha\text{H}$  Lys), 4.45-4.27 (m, 1H,  $\text{C}^\alpha\text{H}$  Phe), 3.55-3.34 (m, 4H,  $\text{C}^\alpha\text{H}_2$  Gly,  $\text{C}^\beta\text{H}_2$  Phe), 2.02-1.79 (m, 7H,  $\text{C}^\beta\text{H}_2$  Leu,  $\text{C}^\gamma\text{H}$  Leu,  $\text{C}^\beta\text{H}_2$  Lys,  $\text{C}^\epsilon\text{H}_2$  Lys), 1.62-1.61 (m, 2H,  $\text{C}^\delta\text{H}_2$  Lys), 1.40-1.39 (m, 2H,  $\text{C}^\gamma\text{H}_2$  Lys), 0.65-0.56 (m, 6H,  $\text{C}^{\gamma\gamma'}\text{H}_3$  Leu).

#### Synthesis of $\text{H}_2\text{N-Gln-Thr-Thr-Thr-Trp-Gln-Asp-Pro-Arg-Lys-Gly-CONH}_2$

The peptide was synthesized on  $\text{Fe}_3\text{O}_4@\text{SiO}_2@\text{NH}-(\beta\text{Ala})_2@\text{Rink-Linker-particles}$  and purified using the same protocol as described above. The synthesis yielded in 3.5 mg of the peptide with 71 % purity.

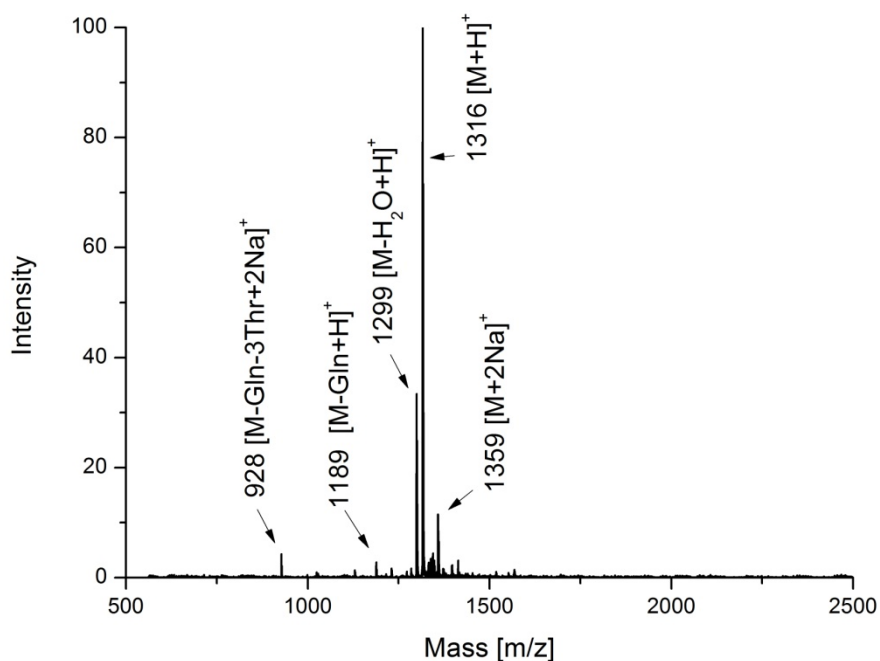


Figure S16. MALDI-spectrum of synthesized undecapeptide H<sub>2</sub>N-Gln-Thr-Thr-Thr-Trp-Gln-Asp-Pro-Arg-Lys-Gly-CONH<sub>2</sub>; M<sub>Th</sub> = 1315.66 g/mol.

- 1 O. Glatter and O. Kratky, *Small angle x-ray scattering*, Academic Press, 1982.
- 2 J. Ilavsky and P. R. Jemian, *Journal of Applied Crystallography*, 2009, **42**, 347.
- 3 G. Beaucage, *Journal of Applied Crystallography*, 1995, **28**, 717.
- 4 G. Beaucage, H. K. Kammler, R. Mueller, R. Strobel, N. Agashe, S. E. Pratsinis and T. Narayanan, *Nature Materials*, 2004, **3**, 370.
- 5 G. Beaucage, H. K. Kammler and S. E. Pratsinis, *Journal of Applied Crystallography*, 2004, **37**, 523.